Advances in Radiation Oncology (2023) **8**, 101128

advances in radiation oncology

www.advancesradonc.org

Scientific Article

Linear Energy Transfer and Relative Biological Effectiveness Investigation of Various Structures for a Cohort of Proton Patients With Brain Tumors

Ana Vaniqui, PhD,* Femke Vaassen, MSc, Dario Di Perri, PhD, Daniëlle Eekers, PhD, Inge Compter, PhD, Ilaria Rinaldi, PhD, Wouter van Elmpt, PhD, and Mirko Unipan, PhD

Department of Radiation Oncology (MAASTRO), GROW School for Oncology, Maastricht University Medical Centre, Maastricht, The Netherlands

Received 21 September 2022; accepted 31 October 2022

Abstract

Purpose: The current knowledge on biological effects associated with proton therapy is limited. Therefore, we investigated the distributions of dose, dose-averaged linear energy transfer (LET_d), and the product between dose and LET_d ($DLET_d$) for a patient cohort treated with proton therapy. Different treatment planning system features and visualization tools were explored.

Methods and Materials: For a cohort of 24 patients with brain tumors, the LET_d, $DLET_d$, and dose was calculated for a fixed relative biological effectiveness value and 2 variable models: plan-based and phenomenological. Dose threshold levels of 0, 5, and 20 Gy were imposed for LET_d visualization. The relationship between physical dose and LET_d and the frequency of LET_d hotspots were investigated.

Results: The phenomenological relative biological effectiveness model presented consistently higher dose values. For lower dose thresholds, the LET_d distribution was steered toward higher values related to low treatment doses. Differences up to 26.0% were found according to the threshold. Maximum LET_d values were identified in the brain, periventricular space, and ventricles. An inverse relationship between LET_d and dose was observed. Frequency information to the domain of dose and LET_d allowed for the identification of clusters, which steer the mean LET_d values, and the identification of higher, but sparse, LET_d values.

Conclusions: Identifying, quantifying, and recording LET distributions in a standardized fashion is necessary, because concern exists over a link between toxicity and LET hotspots. Visualizing $DLET_d$ or dose $\times$ LET_d during treatment planning could allow for clinicians to make informed decisions.

Introduction

The decreased integral dose of ion therapy with respect to photon therapy, combined with recent technological advances, contributed to the significant growth of particle treatments in the last decades. Physically, the finite range of protons and the Bragg peak, with a sharp dose falloff after the target volume, enables better organ-at-risk

Sources of support: Dr Di Perri is supported by a grant from Fondation Saint-Luc, Belgium.

Disclosures: The authors declare that they have no known competing financial interests or personal relationships that could have appeared to influence the work reported in this paper.

Data sharing statement: Research data are stored in an institutional repository and will be shared upon request to the corresponding author.

*Corresponding author: Ana Vaniqui, PhD; E-mail: ana.vaniqui@maastro.nl

https://doi.org/10.1016/j.adro.2022.101128

(OAR) sparing and conformal dose around the target. Biologically, protons cause cellular damage more effectively than photons. Therefore, a conversion factor, relative biological effectiveness (RBE), is used for treatment and comparison between modalities.[1] However, biological effects of proton therapy (PT), in particular those associated with RBE, are less understood than those of photons, triggering discussions on its intrinsic uncertainty.[2-4]

Current clinical practice bases treatments on physical dose and assumes a spatially invariant average RBE value of 1.1.[1] Extensive experimental evidence shows that RBE is in fact variable, dependent on tissue, dose, radiation quality, and other parameters.[5-7] For the clinical energy range, RBE and linear energy transfer (LET), a nonstochastic quantity used to characterize the quality of a beam, present a monotonic correlation, which increases toward the distal edge of the Bragg peak, reaching a maximum at the falloff region. As energy decreases, energy deposition occurs more densely around the protons' tracks, which causes more confined and complex damage.[4,8]

Several phenomenological RBE models exist but present high uncertainties and large variability when compared against each other.[6,9-11] Although a constant average value allows for ubiquitous treatment standardization and disregards RBE uncertainties, neglecting RBE variation might lead to the underestimation of normal tissue complication probability, because highly modulated fields may result in inhomogeneous LET distributions.[12,13] Some studies have also suggested a correlation between late normal tissue toxicity and LET hotspots.[14-18]

LET is defined at a point and describes the average energy transfer from electronic interactions per unit length traveled by charged primary particles.[19,20] Unrestricted LET is equivalent to electronic stopping power, representing energy loss.[19] Dose-averaged LET (LET_d) is a frequently used quantity that considers the stopping power of each individual particle, weighted by its contribution to the local dose.[21,22] LET_d combines different beam qualities, contributing to damage in a single value, and can be used as a predictor for RBE,[23] considering a suggested LET-RBE linear dependence.[24-27] To avoid RBE uncertainty while reducing biological variability in treatment planning, metrics based on computable physical parameters (eg, dose and LET-RBE dependence [as a proxy for response]) have been suggested (eg, product between dose and LET_d [$DLET_d$]).[25,26,28]

In this retrospective study, we investigated the distributions of LET_d, dose (with different RBE models) and $DLET_d$ in a cohort of patients with brain tumors treated between 2019 and 2020 at our institute. Distributions were quantified and analyzed focusing on hotspots adjacent to the clinical target volumes (CTVs) and inside the OARs. The Monte Carlo (MC) engine from our treatment planning system (TPS) was used for all calculations. Although common practice, judging a physical dose is less intuitive for LET_d distributions. The lack of knowledge and experience with this quantity (and its units) pose an additional challenge. To interpret these results, we propose various visualization tools to improve the perception and acquaintance regarding the relationship between treatment planning dose and LET_d distribution.

Methods and Materials

Cohort of neurologic patients

A cohort of 24 patients with brain tumors who received PT between September 2019 and July 2020 was selected for this study. Institutional review board approval (W-210700059) was obtained for this retrospective analysis. Table 1 presents the characteristics of the cohort and treatment planning parameters.

The MC algorithm of RayStation (RaySearch, Sweden) was used for dose calculations with uncertainty set to 1%. All plans were robustly optimized (voxel-wise-minimum-maximum)[29] with range uncertainty set to 3% and universal uncertainty to 1 mm. The TPS optimization for our Mevion S250i Hyperscan PT system (Mevion, Littleton, MA) allows for a number of proximal and distal energy layers to be set. CTV coverage was evaluated on the voxel-wise-minimum and -maximum doses to OAR and on the voxel-wise-maximum and mean doses on the nominal plan, considering constraints according to Lambrecht et al.[30]

Contouring

Target volumes were delineated by experienced radiation oncologists according to national guidelines and OARs according to the European Particle Therapy Network neurocontouring atlas.[31] The periventricular space (PVS) and brain ventricles were also included in this analysis, although not yet contoured at our clinical practice. Besides the CTV, a selection of critical OARs for dosimetric analysis included the brain, brain stem, chiasm, pituitary, left and right (LR) optic nerve, LR cochlea, LR cornea, LR hippocampus, LR lacrimal gland, LR lens, and LR retina. The OAR contours, dose, RBE, and LET distributions were extracted from the TPS for further statistical analysis.

LET and RBE calculations

LET_d, $DLET_d$, and RBE were calculated using the Raystation-9AR-IONPG-Research with the MC engine commissioned for our Mevion system and in-house

Table 1 Cohort description, including number of patients, treatment parameters, tumor type, and location

Patients				Treatment			
Total number			24	**Prescription**	**Dose, Gy**	**Fractions**	**Incidence**
					50.4	28	75.0%
Female			54.2%		54	30	4.2%
Male			45.8%		59.4	33	20.8%
Average age and range, y			44.5 (24-61)	**Number of beams**		3	75.0%
Pathology			95.8%			4	25.0%
Chemotherapy			75.0%	**Dose per fraction, Gy**			1.8
Treatment time, d			40.8 (37-50)	**Distal layers for Monte Carlo optimization**			3
Tumor							
			Central nervous system WHO grade		**Location**	Frontal	62.5%
Type	Oligodendroglioma	37.5%	II (67%), III (33%)			Parietal	12.5%
	Astrocytoma	37.5%	II (100%)			Temporal	12.5%
	Craniopharyngioma	4.2%	II (100%)			Overlapping	12.5%
	Meningioma	20.8%	I (20%), II (20%)		**Laterality**	Right	50.0%
			60%: no pathology available			Left	45.8%
						Midline	4.2%
WHO Eastern Cooperative Oncology Group performance status							
During radiation therapy	**0**	**1**	**2**	**After radiation therapy**	**0**	**1**	**2**
	27.4%	64.0%	8.6%		30.0%	64.0%	6.0%

Abbreviation: WHO = World Health Organization.

Values were calculated considering the entire study population. The performance status grades from the WHO Eastern Cooperative Oncology Group correspond to (0) fully active, normal; (1) symptomatic and ambulatory, cares for self; and (2) ambulatory >50% of the time; occasional assistance needed.

developed scripts. LET_d, the unrestricted mass stopping power scored in the medium and normalized to unity density, was calculated according to:

$$LET_d(z) = \frac{\sum_i \int_0^\infty S_{el}^i(E) D^i(E,z) dE}{\sum_i \int_0^\infty D^i(E,z) dE} \quad (1)$$

where S_{el}^i is the unrestricted electronic stopping power, D^i the dose of the ion type i, E the kinetic energy of the ion, z the position of the ion, and i the ion type. LET_d was computed for primary and secondary protons with its maximum displayed value set to 50 keV/μm. LET_d was calculated for all dose levels within the voxelized geometry and, because high LET_d at low planning doses is not clinically relevant, 3 dose threshold levels were defined at 0, 5, and 20 Gy. Here, LET_d was calculated for the voxels with a dose value above the threshold, otherwise LET_d was set to 0. $DLET_d$ was computed through the voxel-wise product between the planning dose and LET_d distribution through scripting within the TPS.

For the RBE calculation, 2 models were investigated (Unkelbach [UNK][26] and McNamara [MCN][7]), with the $(\alpha/\beta)_x$ set to 2 Gy and fixed to all voxels. Although UNK is a dose-scaling, nontissue, dependent model, MCN is a phenomenological model that considers all published RBE experimental measurements up to 2014.

Visualizing distributions

For each patient, the 3-dimensional distributions of physical dose with RBE of 1.1 ($RBE_{1.1}$), UNK and MCN RBE maps and weighted dose, LET_d (dose threshold of 0, 5, and 20 Gy), and $DLET_d$ were generated. The distributions were displayed as auxiliary doses or additional plans within the TPS and further exported and processed through scripting. To visualize and compare distributions of similar quantities, raincloud plots were chosen to provide a transparent visualization of raw distributions combined with probability density and statistics.[32] Bivariate histograms were used to map the relationship between physical dose and LET_d and to highlight the frequency of the hotspots.

Results

RBE, LET_d, and $DLET_d$ were calculated for all patients considered in the cohort.

RBE models

Considering the entire population, MCN presented the highest dose values for OARs, followed by UNK and $RBE_{1.1}$ (Fig. 1). For small structures (eg, chiasm and pituitary gland), an average increase of 19.3% and 25.5% for MCN and 5.2% and 7.3% for UNK, respectively, was identified with respect to $RBE_{1.1}$. For larger structures and the CTV, the difference was less pronounced (eg, brain and PVS: 2.9% and 18.3% for MCN, and 1.0% and 4.8% for UNK, respectively). The mean $RBE_{1.1}$, MCN, and UNK CTV doses were 52.1 Gy (±2.5; range, 41.8-63.5), 52.1 Gy (±2.7; range, 42.4-67.6), and 57.2 Gy (±3.1; range, 46.5-75.7), respectively.

LET_d calculations

The choice of a clinically meaningful dose threshold caused a substantial effect on the LET_d results. The avoidance of voxels with lower doses greatly affected the LET_d distribution in OARs. When no dose limit was imposed, the distribution was steered toward higher LET_d values, which arose from very low treatment doses (red plots [LET0] of Fig. 2). LET5 and LET20 showed that the threshold magnitude affects the mean LET values. Differences were found up to 26.0% (for the retina).

Although the largest average values were found for the chiasm (LET20: 3.1 ± 1.8 keV/μm; LET5: 3.5 ± 1.8 keV/μm; LET0: 4.4 ± 2.1 keV/μm) and pituitary (LET20: 3.0 ± 2.2 keV/μm; LET5: 4.0 ± 2.0 keV/μm; LET0: 4.8 ± 1.7 keV/μm), the maximum LET_d values were identified in the brain, PVS, and ventricles (LET20: 8.6 ± 1.0 keV/μm; LET5: 10.5 ± 1.5 keV/μm). For LET0, the maximum values coincided with the maximum displayed setting of 50 keV/μm for most structures.

Besides the skin, brain, CTV, PVS, and ventricles, when a dose threshold was imposed, most patients exhibited 0 LET distributions for all other structures (eg, for left lacrimal gland, retina, and cochlea). Only 2 patients presented LET distributions >0, and the entire cohort presented a 0 LET distribution for the spinal cord, lenses, and corneas. When considering all OARs, a mean organ-wise LET_d of 0.8 keV/μm (±0.9; range, 0.0-3.1 keV/μm), 1.26 keV/μm (±1.11; range, 0.0-4.0 keV/μm), and 4.12 keV/μm (±0.72; range, 2.9-5.6 keV/μm) was found for the highest to lowest dose threshold and a consistent value of 2.51 keV/μm (±0.4; range, 1.2-6.0 keV/μm) for the CTV, independent of the threshold.

Dose-LET_d relationships

Different dose cutoffs affected $DLET_d$ distributions to a lesser extent, because this quantity prevents high LET spikes in low-dose regions (Fig. 3). When considering $DLET_d$ values >0 (Fig. 3), for the 20 Gy threshold, mean $DLET_d$ results ranged from 74 Gy·keV/μm (±27; range, 32-143 Gy·keV/μm) to 174 Gy·keV/μm (±28; range, 69-267 Gy·keV/μm) for the right lacrimal gland and brain stem, respectively. The maximum values were found

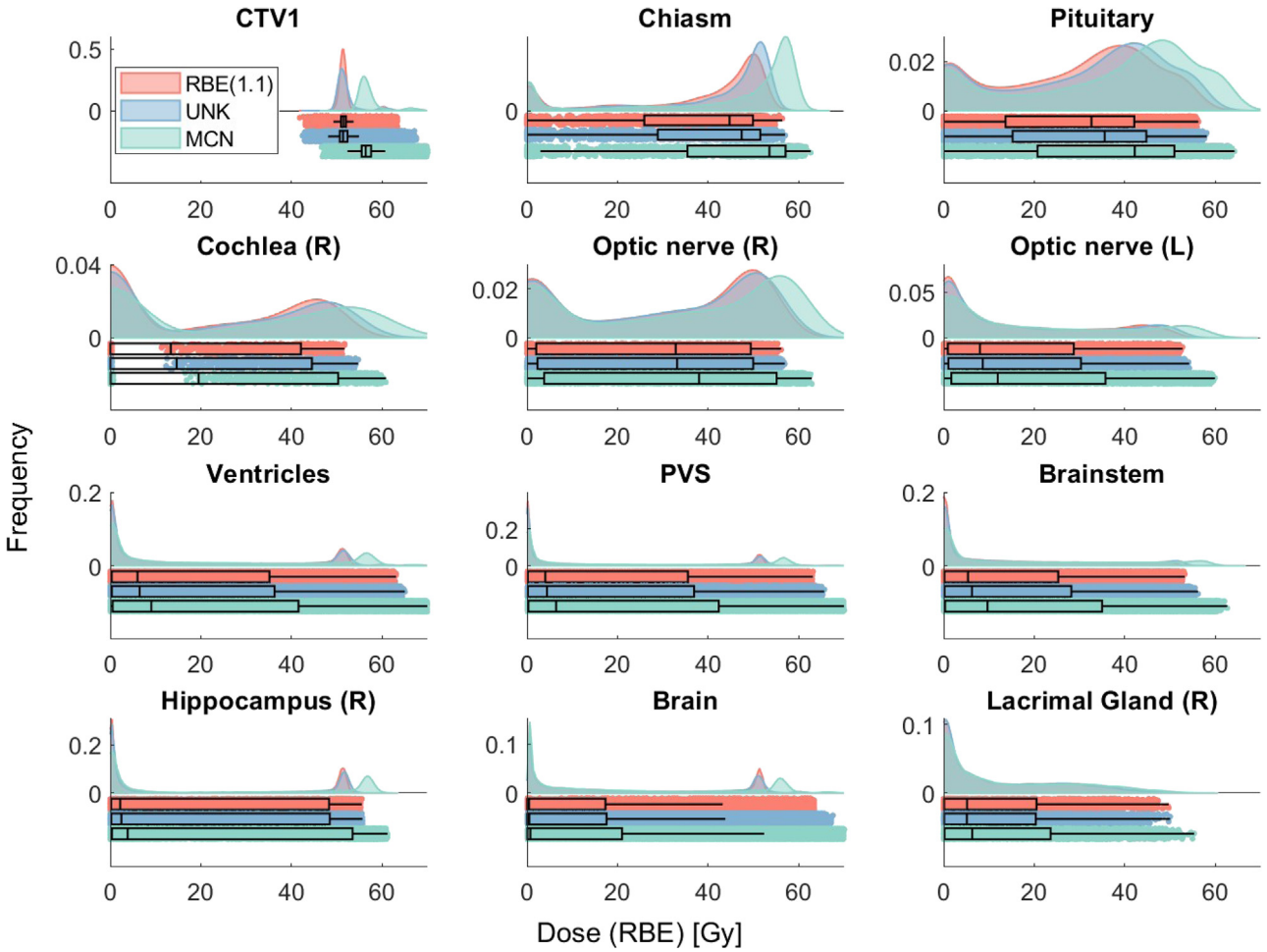

Figure 1 Relative biological effectiveness (RBE) dose distributions for a selection of organs at risk, calculated using the constant clinical factor of 1.1 (red), McNamara's model (green; α/β of 2 Gy), and Unkelbach's model (blue). Both histograms and bars present the frequency distribution (differential dose and number of voxels per unit of RBE dose). The boxplots show the interquartile range, median, and outliers.

in the PVS, ventricles, brain, skin, and CTV (306 ± 28 to 354 ± 45 Gy·keV/μm).

Throughout the population, an inverse relationship between LET_d and dose was observed. For some structures (eg, chiasm and pituitary), this relationship was more evident (Fig. 4). These structures abut the CTV and several distal layers are used for treatment optimization; thus, higher LET_d regions may arise beyond the OARs in regions not considered during optimization, such as the PVS.

Figure 4B presents an overview of the relationship between LET_d and dose. Additional frequency information was visualized using the dose and LET_d, on a structure (Fig. 5) or patient (Fig. 6) basis. Such enhanced visualization allows for the identification and interpretation of clusters, which steer the mean LET_d values and identification of the higher, but sparse, LET_d values. For this cohort (Fig. 5), LET_d values exceeding 6 keV/μm were only present for half of the investigated OARs and always <5% of the structure's voxels (1.2% on average). Although the pituitary presented 4.2% of its voxels >6 keV/μm (mean, 6.3 ± 0.2; range, 6.0-6.9 keV/μm, corresponding to a mean dose of 27.2 ± 3.5 keV/μm), the PVS and brain presented with 0.7% (mean, 6.5 ± 0.5, 6.0-8.6; mean dose, 29.2 ± 5.3 keV/μm) and 0.2% (mean, 6.5 ± 0.4, 6.0-8.6; mean dose, 28.4 ± 5.1 keV/μm), respectively.

As a patient-based approach, planning quality for individual anatomies promoted an organ-based visualization of LET gradients (Fig. 6). Similar histograms associated with each OAR (eg, PVS) promoted the identification of variation within the cohort and the identification of outliers and higher LET_d distributions.

Discussion

An approach was presented for visualization and explorative investigations of RBE-weighted doses, LET_d,

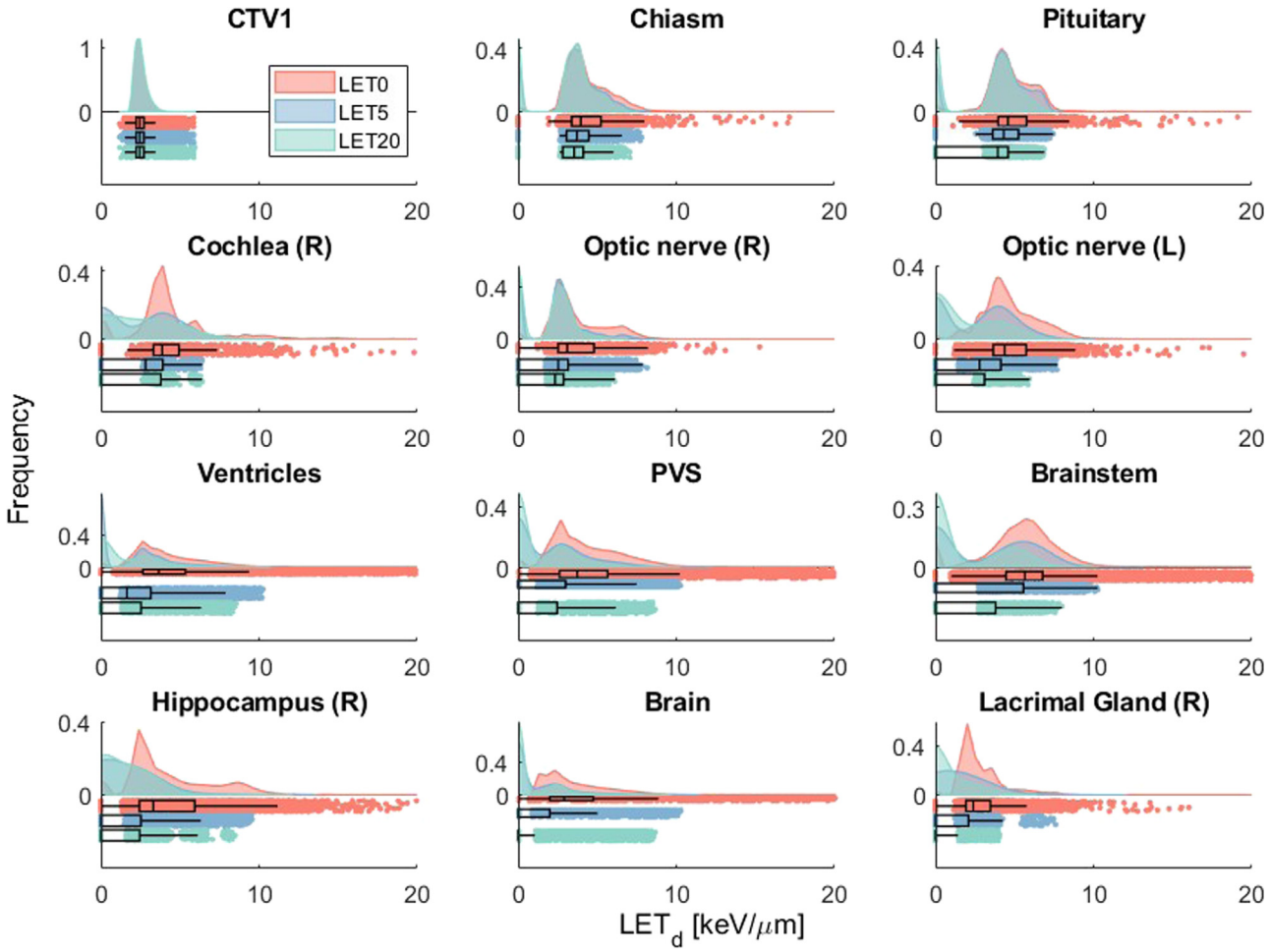

Figure 2 Dose-averaged linear energy transfer (LET_d) distributions for a selection of organs at risk, calculated using dose thresholds of 0 Gy (red), 5 Gy (blue), and 20 Gy (green). Both histograms and bars present the frequency distribution, or the number of voxels per unit of LET_d value. The boxplots show the interquartile range, median, and outliers according to the individual distribution.

and $DLET_d$ for multiple OARs of patients with tumors in different regions of the brain. For the considered RBE models, MCN values were consistently higher than UNK, which has been shown in other studies.[6,16] For brain structures associated with cognition, the average RBE values of 1.54 (0.13) and 1.09 (0.02) found for MCN and UNK, respectively, agree with the reported values of 1.21 and 1.09.[16] Although UNK performs LET optimization based on objective functions evaluated for $DLET_d$ (scaled down by a factor and considered as a measure of the additional biological dose caused by high LET), MCN is a variable phenomenological model.

For simplicity and consistency (α/β) was defined as 2 Gy. This assumption possibly affected the MCN results, which predict the highest RBE for low (α/β) values. Moreover, brain tumors likely have high (α/β) values,[33] and variable models[7,34,35] predict large RBE differences when the difference in (α/β) is large between adjacent structures. A recent review reported $(\alpha/\beta)_x$ target values between 3.1 and 12.5 Gy for glioma and 3.3 and 3.8 Gy for meningioma, as well as for OAR endpoints between 2 and 3 for chiasm (loss of vision), optic nerve (neuropathy), and brain (necrosis).[36]

Besides the investigated models, many others exist with various levels of complexity, regression techniques, and experimental data sets. However, the correlation between RBE variation and outcome data are still impaired by a lack of current in vivo data with up-to-date fractionation schedules, modulation techniques, and evidence from randomized clinical trials.[2] Recent reviews highlight considerable variability among models, predominantly in normal tissues.[6,24,36] Moreover, RBE is intrinsically a quantity conceived for comparing radiation qualities. Thus, the conservative clinical recommendation of using the 1.1 constant factor still simplifies clinical routine, ensures tumor control, and promotes clinical consistency and shared experience across the PT field.[5]

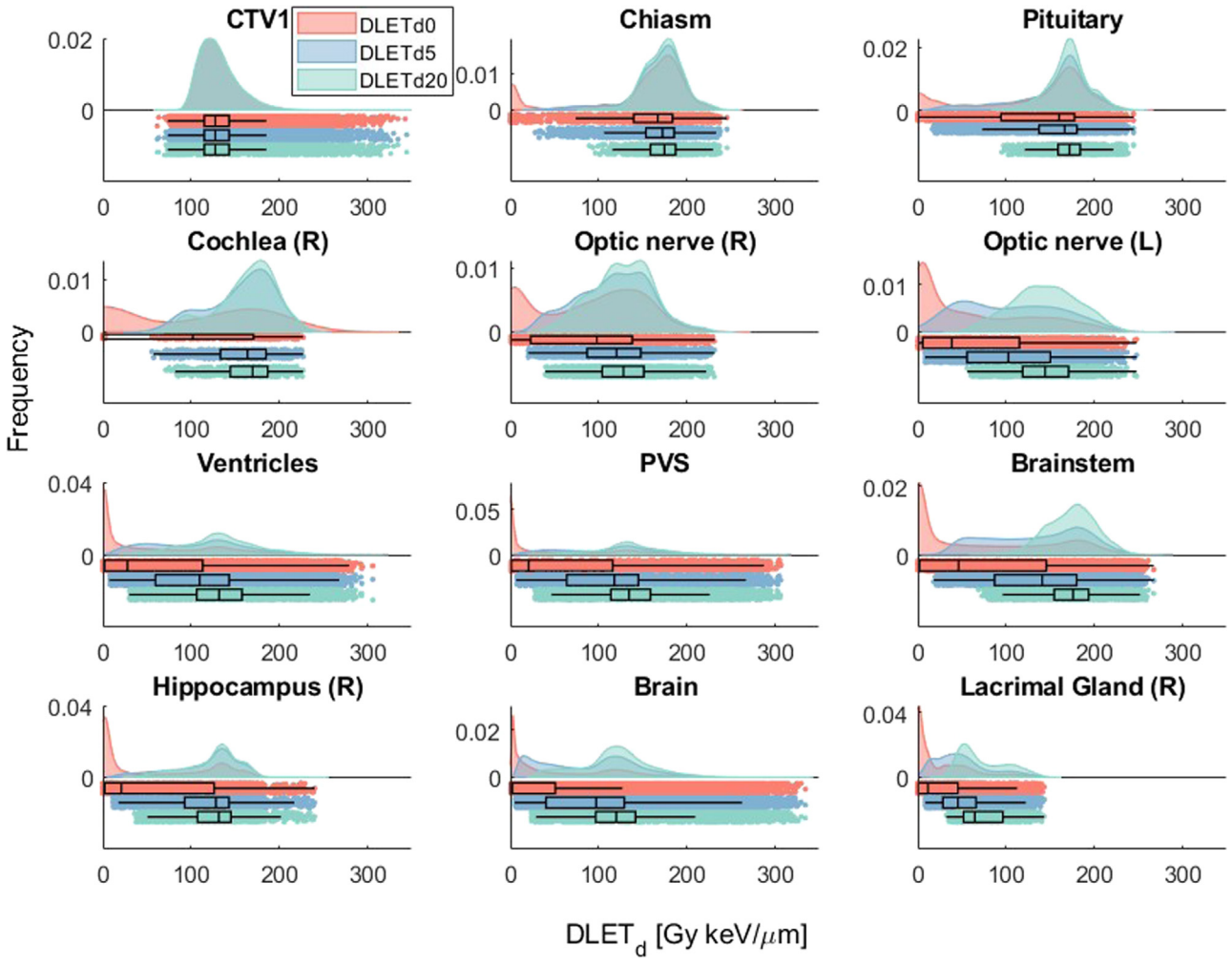

Figure 3 Product between dose and dose-averaged linear energy transfer ($DLET_d$) distributions for a selection of organs at risk, calculated using 0 Gy (red), 5 Gy (blue), and 20 Gy (green) relative biological effectiveness dose threshold. Both histograms and bars present the frequency distribution, or the number of voxels per unit of $DLET_d$ value. The boxplots show the interquartile range, median, and outliers according to the individual distribution.

Although the invariant factor is clinically reasonable, experimental evidence indicates increased RBE toward the distal edge of the treatment field.[1,2,14,33] In this region, as proton energies decrease, denser energy deposition clusters and more complex DNA damage are expected.[21] Therefore, higher LET values and an extension of the treatment range beyond the target are also possible.[34] A thorough RBE review presented average values of 1.1, 1.15, 1.35, and 1.7 at the entrance, center, distal edge, and distal falloff of the spread-out Bragg peak, respectively.[24] This consideration is relevant for neurologic cases, because increased tissue homogeneity, positioning accuracy, less range straggling, and shallower tumors promote sharper dose distributions; thus, OARs close to the target could be affected.[2,35]

A preliminary analysis showed that the majority of patients presented herein reported little or no acute toxicity and normal performance during and up to 2 years after treatment. However, 2 years could be too early to detect any observable toxicities. Although PT radiation-induced brain lesions have been associated with increased RBE and LET values,[17,33,37] comparable results have been observed for photon treatments, where the LET effect is much less pronounced.[38-40] Further outcome investigations (eg, periodic functional imaging to track changes in brain anatomy), along with cognitive tests for protons, photons, and correlation with LET_d distributions for large patient cohorts selected with specific criteria could improve the current knowledge. However, a full analysis of the current visualization techniques related to treatment side effects is outside of the scope of the current study and subject to further analysis.

Additionally, there is a lack of consensus or guidelines on what configures LET hotspots. LET values of typical beam arrangements have been reported of approximately 2 to 4 keV/μm in the center of the beam, from the

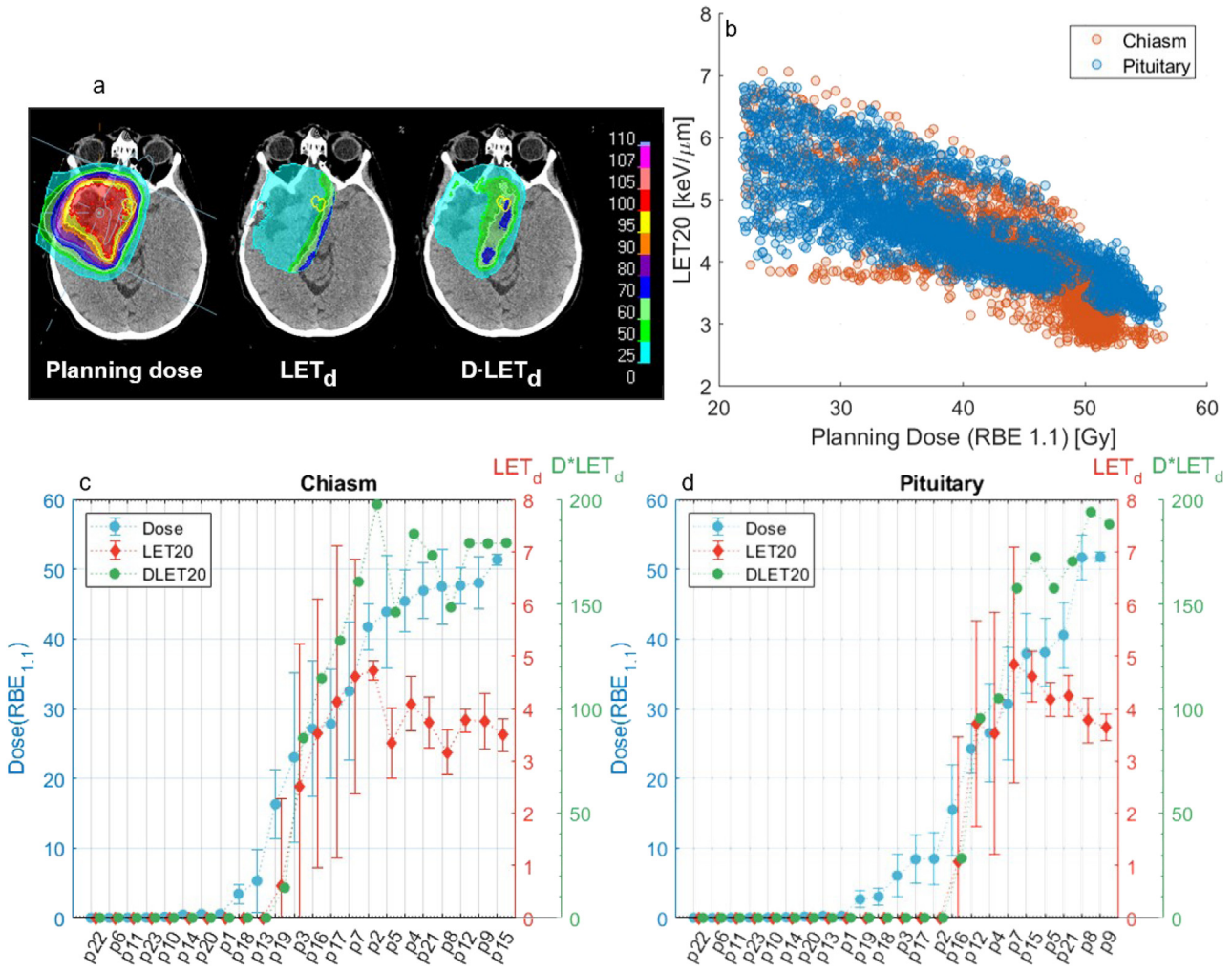

Figure 4 (A) Example patient with planning dose, dose-averaged linear energy transfer (LET_d), and product between dose and dose-averaged linear energy transfer ($DLET_d$) distributions with the optic chiasm contoured in yellow. (B) Distribution of dose and LET_d values for the chiasm (orange) and pituitary (blue) for all patients (N = 24) in the study. (C, D) Relationship between mean values of dose, LET_d, and $DLET_d$ (for dose threshold of 20 Gy) for the chiasm and pituitary gland. Dose, LET_d, and $DLET_d$ are represented by the blue, red, and green axes, respectively.

proximal to distal target regions, and >10 keV/μm at the distal falloff.[24,35] However, intensity modulated PT delivers highly inhomogeneous dose distributions outside of the target volume, and dose–response data has been reported for a broad range of LET values, which may not consider dose threshold and incorporate low-energy protons with increased LET.[41]

Although high LET values in low-dose regions are reported to not be clinically relevant,[24,42] to the best of our knowledge, no agreement exists on cutoff doses below which no LET should be evaluated. MC methods unavoidably result in a number of voxels with few interactions and high statistical uncertainty. The choice of a 0-Gy threshold exemplifies this effect in low-dose and out-of-field regions. In this study, different thresholds were evaluated (Fig. 2) and, considering prescription dose and OAR constraints, the highest threshold (20 Gy) is likely to be more clinically relevant. Individual OAR radiosensitivity could also be considered to specify a constraint, because 20 Gy can be prohibiting for some OARs (eg, eye lenses). On the other hand, as we also consider stochastic nature radiation effects and a general unfamiliarity with underlying causes of late effects, a threshold becomes relevant for instant visualization, but full data should be preserved for future outcome analyses.

The chiasm (3.1 ± 1.8 keV/μm) and pituitary (3.0 ± 2.2 keV/μm) presented the largest averaged LET_d values. For these and other small structures (eg, optic nerve and cochlea), decreasing LET_d values with increasing dose were observed. Due to the limitations of this study (eg, cohort size and heterogeneous tumor sites and beam orientations), different OARs, and especially the smaller ones, received little or no dose. This aspect was considered in the statistical analysis but does not explain the larger

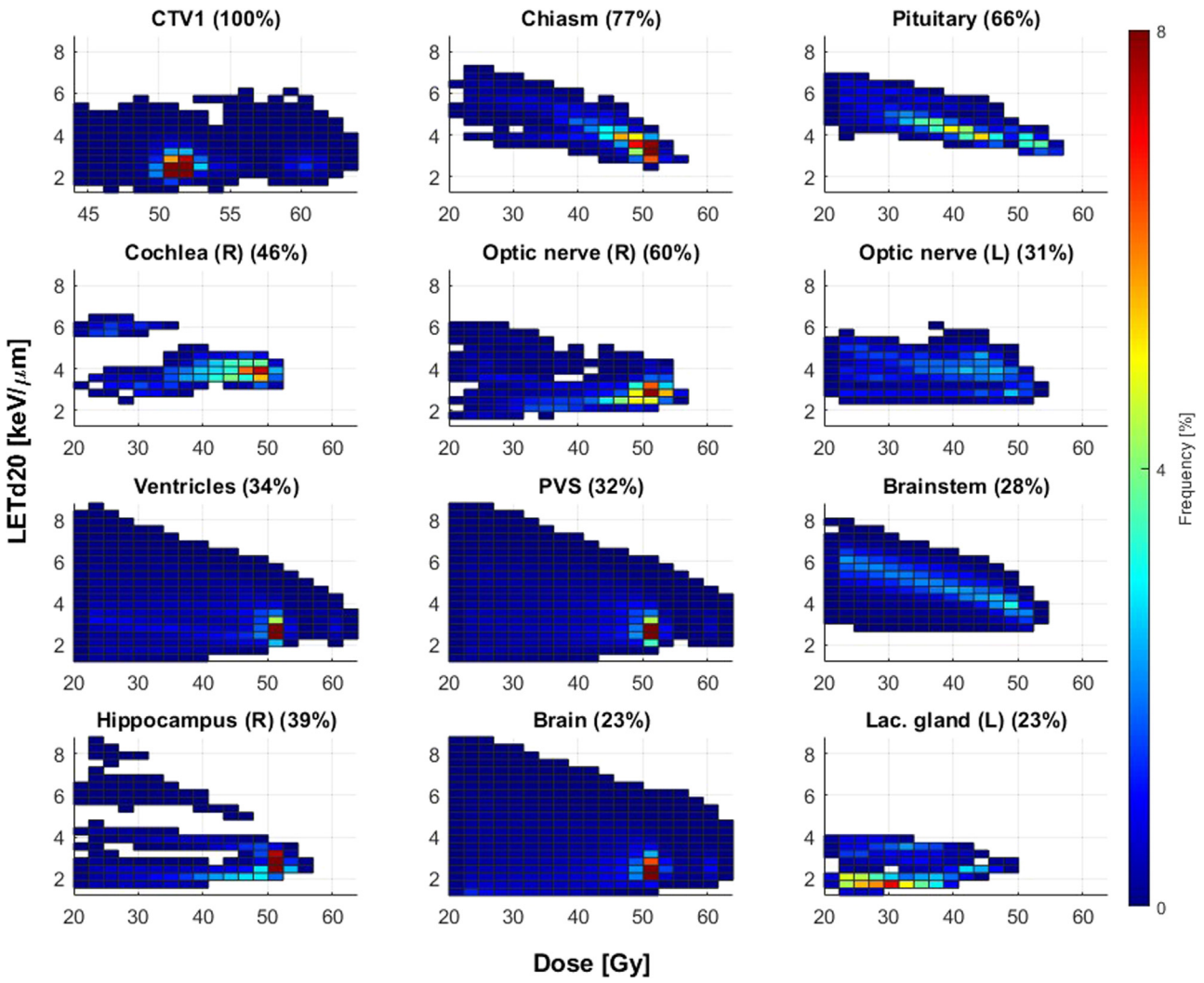

Figure 5 Dose and dose-averaged linear energy transfer (LET_d) histograms of a selection of investigated structures for a single patient. Dose and LET_d values are represented on the x- and y-axes, respectively, for each subplot. Next to each structure name, the percentage of voxels >0 is indicated, as used for the graph. The color bar on the right indicates the frequency in the same scale for all plots.

differences found for smaller structures compared with the larger structures. Multiple distal layers are used during treatment optimization; thus, high LET values possibly fall beyond critical structures when they adjoin the CTV. These regions likely coincide with the ventricles and PVS, for which no clinical dose constraints are considered during optimization and where the maximum global LET_d values were identified (8.6 ± 1.0 keV/μm).

Different studies have associated late radiation-induced brain lesions in regions of increased LET_d, RBE, and radiosensitivity at the PVS.[14,15,43] Our study also highlights this structure, considering that treatment planning strategies to neutralize increased RBE (or LET) focus on placing the distal edge outside OARs, which coincide with the periventricular region. A recent survey showed that, even though all European PT centers use a constant RBE factor of 1.1, they also apply measures to counteract variable RBE effects (ie, avoid beams stopping inside or in front of an OAR)[44], disregarding the PVS.

Considering the uncertainties on RBE models and the difficult interpretation of LET alone, the LET–RBE dependence has been used as a proxy for biological response (eg, in the product between dose and LET).[2,6,14,25,26,45] Logically, a dose cutoff is not so relevant when the product itself attends the effect of LET spikes in low-dose regions. To avoid LET overestimation, McMahon et al. added a factor to LET-weighted doses, which performed well compared with several RBE models.[25] Although a thorough analysis might still be necessary, this factor represents a simple approach to readily identify high LET without the influence of low-dose values. Additional tools to promote a better visualization of the relationship between LET and dose are also helpful to estimate its magnitude, identify hotspots, and compare

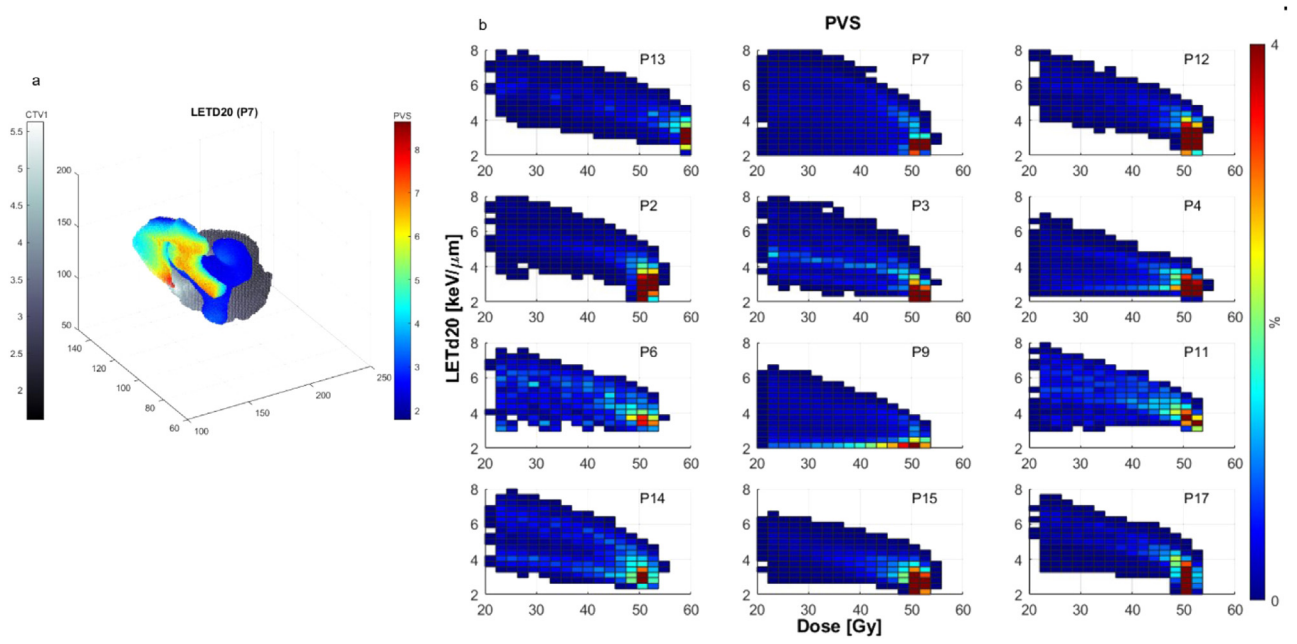

Figure 6 (A) Clinical target volume (CTV; gray color map) and periventricular space (PVS; multiple colors) dose-averaged linear energy transfer (LET_d) distribution spatial representation. (B) Dose–LET_d histograms of the PVS for different patients. Dose and LET_d values are represented on the x- and y-axes, respectively, for each subplot. The color bar on the right indicates the frequency in the same scale for all plots.

and characterize treatment planning quality considering inter- and intrapatient LET distributions.

The heat maps presented in this study show a low frequency of higher LET values in regions restricted to lower doses below known tolerances. This effect should become less pronounced when different treatment uncertainties are also considered, such as range straggling, imaging uncertainty, and treatment variation in anatomy, positioning, motion, setup, dose distribution, and tissue heterogeneity.[13,33,46] Nevertheless, LET-guided robust optimization is a growing field that focuses on maximizing LET to the target while minimizing LET in OARs, minimally affecting the clinical goals of the treatment plan.[15,42,47-50] This approach is supported by the TG-256 study, which suggests LET assessment and LET-based optimization.[1] Besides optimization, adaptation of treatment techniques (eg, splitting the target) has also been reported.[51,52]

Because the effect of high LET in normal tissue is not fully understood, there is growing concern over its management, as LET visualization and optimization tools are not yet fully implemented in clinical TPSs. This study presents visualization strategies to quantify OAR and patient treatment quality based on the relationship between dose and LET. Investing in such visualization tools and standardization of LET reporting is necessary[41] and could assist clinicians to identify and characterize hotspots in regions susceptible to damage, as well as examine LET distributions for new techniques (eg, proton arc).

Conclusion

From the analysis of RBE models, LET_d, and $DLET_d$ derived from our TPS for patients with brain tumors, strategies were proposed to assess treatment quality considering regions with increased LET_d. For clinical practice, identifying, quantifying, and recording LET distributions is important, because concern exists over a link between normal tissue toxicity and LET hotspots. LET calculation and reporting requires standardization. The lack of a uniform approach was exemplified by the effect of establishing dose thresholds, which modifies LET reporting, and should be considered with a clinical rationale. Visualizing the dose and LET_d space during treatment planning can provide a prompt check of high-LET regions and allow for the clinician to decide if changes in the planning technique are necessary. Finally, systematically acquiring clinically relevant data for treatment and outcomes is necessary for a robust clinical analysis and comparison with photon treatments, as well as provide guidance on how to incorporate this information in clinical decision making.

Supplementary materials

Supplementary material associated with this article can be found in the online version at doi:10.1016/j.adro.2022.101128.

References

1. Paganetti H, Blakely E, Carabe-Fernandez A, et al. Report of the AAPM TG-256 on the relative biological effectiveness of proton beams in radiation therapy. *Med Phys*. 2019;46:e53-e78.
2. Luhr A, von Neubeck C, Pawelke J, et al. Radiobiology of proton therapy: Results of an international expert workshop. *Radiother Oncol*. 2018;128:56-67.
3. Zhang J, Si J, Gan L, et al. Harnessing the targeting potential of differential radiobiological effects of photon versus particle radiation for cancer treatment. *J Cell Physiol*. 2021;236:1695-1711.
4. Sorensen BS, Bassler N, Nielsen S, et al. Relative biological effectiveness (RBE) and distal edge effects of proton radiation on early damage in vivo. *Acta Oncol*. 2017;56:1387-1391.
5. Mohan R, Peeler CR, Guan F, et al. Radiobiological issues in proton therapy. *Acta Oncol*. 2017;56:1367-1373.
6. Rorvik E, Fjaera LF, Dahle TJ, et al. Exploration and application of phenomenological RBE models for proton therapy. *Phys Med Biol*. 2018;63: 185013.
7. McNamara AL, Schuemann J, Paganetti H. A phenomenological relative biological effectiveness (RBE) model for proton therapy based on all published in vitro cell survival data. *Phys Med Biol*. 2015; 60:8399-8416.
8. Chaudhary P, Marshall TI, Perozziello FM, et al. Relative biological effectiveness variation along monoenergetic and modulated Bragg peaks of a 62-MeV therapeutic proton beam: A preclinical assessment. *Int J Radiat Oncol Biol Phys*. 2014;90:27-35.
9. Stewart RD, Carlson DJ, Butkus MP, et al. A comparison of mechanism-inspired models for particle relative biological effectiveness (RBE). *Med Phys*. 2018;45:e925-e952.
10. McMahon SJ. Proton RBE models: Commonalities and differences. *Phys Med Biol*. 2021;66:04NT02.
11. McMahon SJ, Prise KM. Mechanistic modelling of radiation responses. *Cancers (Basel)*. 2019;11:205.
12. Oden J, DeLuca Jr PM, Orton CG. The use of a constant RBE = 1.1 for proton radiotherapy is no longer appropriate. *Med Phys*. 2018;45:502-505.
13. Grassberger C, Paganetti H. Varying relative biological effectiveness in proton therapy: Knowledge gaps versus clinical significance. *Acta Oncol*. 2017;56:761-762.
14. Bauer J, Bahn E, Harrabi S, et al. How can scanned proton beam treatment planning for low-grade glioma cope with increased distal RBE and locally increased radiosensitivity for late MR-detected brain lesions? *Med Phys*. 2021;48:1497-1507.
15. Bahn E, Bauer J, Harrabi S, et al. Late contrast enhancing brain lesions in proton-treated patients with low-grade glioma: Clinical evidence for increased periventricular sensitivity and variable RBE. *Int J Radiat Oncol Biol Phys*. 2020;107:571-578.
16. Otterlei OM, Indelicato DJ, Toussaint L, et al. Variation in relative biological effectiveness for cognitive structures in proton therapy of pediatric brain tumors. *Acta Oncol*. 2021;60:267-274.
17. Peeler CR, Mirkovic D, Titt U, et al. Clinical evidence of variable proton biological effectiveness in pediatric patients treated for ependymoma. *Radiother Oncol*. 2016;121:395-401.
18. Bertolet A, Abolfath R, Carlson DJ, et al. Correlation of LET with MRI changes in brain and potential implications for normal tissue complication probability for patients with meningioma treated with pencil beam scanning proton therapy. *Int J Radiat Oncol Biol Phys*. 2021;112:237-246.
19. International Commission on Radiation Units and Measurements. Report 16. *J ICRU*. 2016:os9.
20. Thomas DJ. ICRU report 85: Fundamental quantities and units for ionizing radiation. *Radiat Protect Dosim*. 2012;150:550-552.
21. Wilkens JJ, Oelfke U. Analytical linear energy transfer calculations for proton therapy. *Med Phys*. 2003;30:806-815.
22. Guan F, Peeler C, Bronk L, et al. Analysis of the track- and dose-averaged LET and LET spectra in proton therapy using the Geant4 Monte Carlo code. *Med Phys*. 2015;42:6234-6247.
23. Engeseth GM, He R, Mirkovic D, et al. Mixed effect modeling of dose and linear energy transfer correlations with brain image changes after intensity modulated proton therapy for skull base head and neck cancer. *Int J Radiat Oncol Biol Phys*. 2021;111:684-692.
24. Paganetti H. Relative biological effectiveness (RBE) values for proton beam therapy. Variations as a function of biological endpoint, dose, and linear energy transfer. *Phys Med Biol*. 2014;59:R419-R472.
25. McMahon SJ, Paganetti H, Prise KM. LET-weighted doses effectively reduce biological variability in proton radiotherapy planning. *Phys Med Biol*. 2018;63: 225009.
26. Unkelbach J, Botas P, Giantsoudi D, et al. Reoptimization of intensity modulated proton therapy plans based on linear energy transfer. *Int J Radiat Oncol Biol Phys*. 2016;96:1097-1106.
27. Rucinski A, Biernacka AM, Schulte RW. Applications of nanodosimetry in particle therapy planning and beyond. *Phys Med Biol*. 2021;66:10.
28. Fjaera LF, Li Z, Ytre-Hauge KS, et al. Linear energy transfer distributions in the brainstem depending on tumour location in intensity-modulated proton therapy of paediatric cancer. *Acta Oncol*. 2017; 56:763-768.
29. Korevaar EW, Habraken SJM, Scandurra D, et al. Practical robustness evaluation in radiotherapy—A photon and proton-proof alternative to PTV-based plan evaluation. *Radiother Oncol*. 2019;141:267-274.
30. Lambrecht M, Eekers DBP, Alapetite C, et al. Radiation dose constraints for organs at risk in neuro-oncology; the European Particle Therapy Network consensus. *Radiother Oncol*. 2018;128:26-36.
31. Eekers DBP, Di Perri D, Roelofs E, et al. Update of the EPTN atlas for CT- and MR-based contouring in neuro-oncology. *Radiother Oncol*. 2021;160:259-265.
32. Allen M, Poggiali D, Whitaker K, et al. Raincloud plots: A multi-platform tool for robust data visualization. *Wellcome Open Res*. 2021;4:63.
33. Underwood TSA, Grassberger C, Bass R, et al. Asymptomatic late-phase radiographic changes among chest-wall patients are associated with a proton RBE exceeding 1.1. *Int J Radiat Oncol Biol Phys*. 2018;101:809-819.
34. Durante M, Paganetti H. Nuclear physics in particle therapy: A review. *Rep Prog Phys*. 2016;79: 096702.
35. Grassberger C, Trofimov A, Lomax A, et al. Variations in linear energy transfer within clinical proton therapy fields and the potential for biological treatment planning. *Int J Radiat Oncol Biol Phys*. 2011;80:1559-1566.
36. Paganetti H. Mechanisms and review of clinical evidence of variations in relative biological effectiveness in proton therapy. *Int J Radiat Oncol Biol Phys*. 2022;112:222-236.
37. Haas-Kogan D, Indelicato D, Paganetti H, et al. National Cancer Institute workshop on proton therapy for children: Considerations regarding brainstem injury. *Int J Radiat Oncol Biol Phys*. 2018; 101:152-168.
38. Bronk JK, Guha-Thakurta N, Allen PK, et al. Analysis of pseudoprogression after proton or photon therapy of 99 patients with low grade and anaplastic glioma. *Clin Transl Radiat Oncol*. 2018;9:30-34.
39. van West SE, de Bruin HG, van de Langerijt B, et al. Incidence of pseudoprogression in low-grade gliomas treated with radiotherapy. *Neuro Oncol*. 2017;19:719-725.
40. Lu VM, Welby JP, Laack NN, et al. Pseudoprogression after radiation therapies for low grade glioma in children and adults: A systematic review and meta-analysis. *Radiother Oncol*. 2020;142:36-42.
41. Kalholm F, Grzanka L, Traneus E, et al. A systematic review on the usage of averaged LET in radiation biology for particle therapy. *Radiother Oncol*. 2021;161:211-221.

42. Traneus E, Oden J. Introducing proton track-end objectives in intensity modulated proton therapy optimization to reduce linear energy transfer and relative biological effectiveness in critical structures. *Int J Radiat Oncol Biol Phys*. 2019;103:747-757.
43. Eulitz J, Troost EGC, Raschke F, et al. Predicting late magnetic resonance image changes in glioma patients after proton therapy. *Acta Oncol*. 2019;58:1536-1539.
44. Heuchel L, Hahn C, Pawelke J, et al. Clinical use and future requirements of relative biological effectiveness: Survey among all European proton therapy centres. *Radiother Oncol*. 2022;172:134-139.
45. McMahon SJ, Prise KM. A mechanistic DNA repair and survival model (Medras): Applications to intrinsic radiosensitivity, relative biological effectiveness and dose-rate. *Front Oncol*. 2021;11: 689112.
46. Niemierko A, Schuemann J, Niyazi M, et al. Brain necrosis in adult patients after proton therapy: Is there evidence for dependency on linear energy transfer? *Int J Radiat Oncol Biol Phys*. 2021;109:109-119.
47. Cao W, Khabazian A, Yepes PP, et al. Linear energy transfer incorporated intensity modulated proton therapy optimization. *Phys Med Biol*. 2017;63: 015013.
48. Giantsoudi D, Grassberger C, Craft D, et al. Linear energy transfer-guided optimization in intensity modulated proton therapy: Feasibility study and clinical potential. *Int J Radiat Oncol Biol Phys*. 2013;87:216-222.
49. Gu W, Ruan D, Zou W, et al. Linear energy transfer weighted beam orientation optimization for intensity-modulated proton therapy. *Med Phys*. 2021;48:57-70.
50. Liu C, Patel SH, Shan J, et al. Robust optimization for intensity modulated proton therapy to redistribute high linear energy transfer from nearby critical organs to tumors in head and neck cancer. *Int J Radiat Oncol Biol Phys*. 2020;107:181-193.
51. Paganetti H, Giantsoudi D. Relative biological effectiveness uncertainties and implications for beam arrangements and dose constraints in proton therapy. *Semin Radiat Oncol*. 2018;28:256-263.
52. Zeng C, Giantsoudi D, Grassberger C, et al. Maximizing the biological effect of proton dose delivered with scanned beams via inhomogeneous daily dose distributions. *Med Phys*. 2013;40: 051708.